Supporting Information

Stability and Phase Transition of Cobalt Oxide Phases by Machine Learning Global Potential Energy Surface

Fan-Chen Kong, Ye-Fei Li, Cheng Shang, Zhi-Pan Liu*

Collaborative Innovation Center of Chemistry for Energy Material, Key Laboratory of Computational Physical Science (Ministry of Education), Shanghai Key Laboratory of Molecular Catalysis and Innovative Materials, Department of Chemistry, Fudan University, Shanghai 200433, China
*Email: zpliu@fudan.edu.cn

Table of Contents

1. Methodology and calculation details

1.1 Stochastic surface walking (SSW) global PES exploration using neural network (NN) potential (SSW-NN method)

The identification of the structures of CoO_x at different compositions asks for a reliable and efficient tool to sample the global potential energy surfaces (PESs). Although density functional theory (DFT) calculations emerged as a reliable tool for PES construction, the poor scaling and the high computational demand intrinsic to electronic structure calculations restricts severely its applications. In this work, we utilize the recently developed SSW-NN method to construct the global PES of CoO_x and to assess their properties. The SSW method is an automated approach to explore the multidimensional PES and its ability to identify the global minimum of complex systems has been demonstrated recently.[1-5] The NN simulation is at least 3~4 orders of magnitude faster than DFT calculation while keeping the accuracy in energy and force comparable with those from DFT. The combination of SSW with NN potential thus allows fasting to obtain the global PES of complex materials. The SSW-NN method to explore PES can be divided into three steps: (a) Global dataset generation based on DFT calculations using selected structures from SSW simulation; (b) NN PES fitting and (c) SSW Global optimization using NN PES.

These steps are iteratively performed until the NN potential is transferable and robust enough to describe the global PES. The initial DFT dataset in the first cycle can be obtained from a short SSW simulation based on DFT. As can be seen from this iterative procedure, there is no need to emphasize particularly testing (or holdout) dataset since in each cycle there are new data to add into the training dataset, which can be utilized to validate NN potential on the fly without causing severely overfitting. We generally repeat this cycle more than 100 cycles with each cycle adding a few hundreds of new data (structures) from DFT. We continuously examine the NN predicted energy for the newly added data: once the predicted RMS error is close to the training accuracy of NN potential in the last cycle, we would consider the NN potential is ready to use for the example systems. The procedure is briefly summarized below (more details can be found in our previous work[6]).

a. Global dataset generation

The global dataset is built iteratively during the self-learning of NN potential. The initial data of the global dataset comes from the DFT-based SSW simulation and all the other data is taken from NN-based SSW PES exploration. In order to cover all the likely compositions of CoO_x, SSW simulations have been carried out for different structures (including bulk, layer/surface and cluster), compositions and atom number per unit cell (~20). Overall, these SSW simulations generate more than 10^7 structures on PES. The final global dataset that is computed from high accuracy DFT calculation contains 42,246 structures, which is detailed in **Table S1**.

Table S1. Structure information of the global dataset generated from first principle calculation. The number of the structures in the global dataset, as distinguished by the chemical formula, the number of atoms (N_{atom}), the type of structures (cluster, bulk, layer) are listed below.

Species	N_{atom}	cluster	layer(surface)	bulk	total
Co16	16	0	0	9093	9093
Co19	19	290	0	0	290

Co21	21	0	273	342	615
Co23	23	0	0	225	225
O1-Co14	15	0	1	1	2
O1-Co18	19	266	0	0	266
O1-Co20	21	0	12	170	182
O2-Co19	21	0	29	6	35
O2-Co20	22	0	35	114	149
O3-Co20	23	0	17	94	111
O4	4	0	94	0	94
O6-Co8	14	0	7	187	194
O7-Co8	15	0	3	171	174
O8-Co6	14	978	0	0	978
O8-Co8	16	574	51	11205	11830
O9-Co12	21	0	0	4	4
O10-Co8	18	0	44	2661	2705
O11	11	0	480	146	626
O11-Co12	23	0	0	7	7
O11-Co16	27	0	0	11	11
O12-Co8	20	277	107	11690	12074
O12-Co12	24	0	0	12	12
O13-Co12	25	0	0	21	21
O14-Co12	26	0	0	39	39
O15-Co12	27	0	0	23	23
O15-Co16	31	0	0	39	39
O16-Co12	28	0	0	2093	2093
O17-Co12	29	0	5	0	5
O18-Co11	29	0	1	1	2
O18-Co12	30	0	1	163	164
O18-Co16	34	0	0	4	4
O20-Co16	36	0	1	75	76
O22-Co20	42	0	2	29	31
O23-Co20	43	0	0	27	27
O24-Co20	44	0	0	19	19
O26-Co20	46	0	0	26	26
total	--	2385	1163	38698	42246

b. NN PES fitting

The NN potential is generated using the method as introduced in our previous work.[6-7] To pursue a high accuracy for PES, we have adopted a large set of power-type structure descriptors (PTSDs), which contains 324 descriptors for every element with only power-type structure descriptors, including 132 2-body, 170 3-body, 22 4-body descriptors. The network utilized involves three-hidden layers (148-80-50-50-1 net). Min-max scaling is utilized to normalization the training data sets. Hyperbolic tangent activation functions were used for the hidden layers, while a linear

transformation was applied to the output layer of all networks. The limited-memory Broyden-Fletcher-Goldfarb-Shanno (L-BFGS) method is used to minimize the loss function to match DFT energy, force and stress. The final energy and force criterions of the root mean square errors are around 12.063 meV/atom and 0.210 eV/ Å respectively. To demonstrate the accuracy of NN PES, we select 64 CoO_x crystal structures to compare the NN results with the DFT calculation results. It has an average energy error of 5.604 meV/atom, which is quite standard for NN potentials and accurate enough for searching the stable structure candidates. The details for the comparison between DFT and NN results can be found in **Table S2**.

Table S2. Benchmark of NN calculations for CoO_x systems as compared with DFT results. Listed data includes the compositions, total atom number (N_{atom}), order parameter with degree l = 4 (OP4), DFT energy, NN energy and energy differences between DFT energy and NN energy (E_{diff}, meV/atom).

Composition[$]	Natom	OP4	DFT-en (eV/atom)	NN-en (eV/atom)	en-diff (meV/atom)
Co20O19_1	39	0.328	-5.604	-5.602	2.084
Co20O19_2	39	0.331	-5.596	-5.600	4.542
Co20O19_3	39	0.330	-5.607	-5.600	7.201
Co20O19_4	39	0.329	-5.602	-5.599	3.002
Co20O19_5	39	0.329	-5.599	-5.602	3.006
Co20O20_1	40	0.337	-5.678	-5.676	2.112
Co20O20_2	40	0.337	-5.675	-5.675	0.006
Co20O20_3	40	0.334	-5.679	-5.675	4.135
Co20O20_4	40	0.336	-5.675	-5.670	5.489
Co20O20_5	40	0.337	-5.666	-5.669	2.937
Co20O21_1	41	0.324	-5.627	-5.633	5.725
Co20O21_2	41	0.332	-5.626	-5.633	7.074
Co20O21_3	41	0.332	-5.621	-5.632	11.052
Co20O21_4	41	0.337	-5.621	-5.631	10.122
Co20O21_5	41	0.337	-5.628	-5.631	2.654
Co20O22_1	42	0.325	-5.613	-5.613	0.211
Co20O22_2	42	0.327	-5.611	-5.608	3.274
Co20O22_3	42	0.326	-5.606	-5.608	1.720
Co20O22_4	42	0.318	-5.605	-5.607	1.056
Co20O22_5	42	0.327	-5.607	-5.606	0.951
Co20O23_1	43	0.333	-5.592	-5.595	3.170
Co20O23_2	43	0.331	-5.586	-5.600	13.610
Co20O23_3	43	0.330	-5.580	-5.598	17.607
Co20O23_4	43	0.326	-5.584	-5.597	13.492
Co20O23_5	43	0.326	-5.582	-5.597	15.478
Co20O24_1	44	0.333	-5.588	-5.588	0.110
Co20O24_2	44	0.319	-5.599	-5.600	1.154
Co20O24_3	44	0.319	-5.610	-5.599	10.539
Co20O24_4	44	0.330	-5.588	-5.598	9.853
Co20O25_1	45	0.349	-5.570	-5.576	6.281

Co20O25_2	45	0.429	-5.576	-5.580	4.765
Co20O25_3	45	0.645	-5.581	-5.582	0.645
Co20O25_4	45	0.434	-5.583	-5.581	2.501
Co20O25_5	45	0.410	-5.588	-5.586	2.486
Co20O25_6	45	0.407	-5.590	-5.583	7.357
Co20O26_1	46	0.332	-5.615	-5.622	7.076
Co20O26_2	46	0.335	-5.620	-5.616	4.259
Co20O26_3	46	0.334	-5.617	-5.617	6.372
Co20O26_4	46	0.334	-5.617	-5.616	0.653
Co20O26_5	46	0.333	-5.620	-5.617	3.834
Co20O27_1	47	0.342	-5.623	-5.621	2.380
Co20O27_2	47	0.348	-5.614	-5.623	8.899
Co20O27_3	47	0.344	-5.625	-5.622	2.447
Co20O27_4	47	0.339	-5.624	-5.622	2.181
Co20O27_5	47	0.339	-5.624	-5.622	2.104
Co20O28_1	48	0.336	-5.629	-5.631	1.808
Co20O28_2	48	0.336	-5.628	-5.630	2.094
Co20O28_3	48	0.348	-5.614	-5.620	6.007
Co20O28_4	48	0.351	-5.611	-5.618	6.614
Co20O28_5	48	0.351	-5.611	-5.616	5.799
Co20O29_1	49	0.325	-5.577	-5.585	7.794
Co20O29_2	49	0.324	-5.576	-5.584	7.941
Co20O29_3	49	0.323	-5.575	-5.582	6.970
Co20O29_4	49	0.338	-5.570	-5.579	9.281
Co20O29_5	49	0.338	-5.563	-5.579	16.143
Co20O30_1	50	0.270	-5.553	-5.552	1.342
Co20O30_2	50	0.268	-5.552	-5.555	3.320
Co12O18_1	30	0.270	-5.554	-5.554	0.673
Co12O18_2	30	0.346	-5.532	-5.539	6.635
Co12O18_3	30	0.384	-5.537	-5.538	1.063
Co12O18_4	30	0.404	-5.519	-5.529	9.700
Co12O18_5	30	0.443	-5.516	-5.517	0.672
Co24O26	50	0.325	-5.612	-5.614	1.972
Co24O31	55	0.309	-5.632	-5.637	4.531

* Mean error between DFT energy and NN energy is 5.604 meV/atom.

[$] CoxOy_z means a unit cell consists of x Co atom and y O atom; z is a serial number to distinguish different structures with same component

c. SSW Global optimization using NN PES

SSW-NN simulation is performed over a wide range of composition and structures, both for the global dataset generation in (a) and for the final production of the phase diagram in Fig. 2, potential energy surface in Fig 4 and Fig S3. For the data in Fig. 2, they are taken from the global minima at each composition of CoO_x as identified from the SSW-NN simulation, where CoO_x with each different composition is simulated in the unit cells of 27 ~ 60 and explored to cover more than

10,000 minima on PES by SSW. Thus, a large variety of structures ranging from crystalline structures to amorphous structures have been obtained from SSW-NN simulation. All the low energy structure candidates from SSW-NN exploration are finally verified by plane wave DFT calculations with high accuracy setups.

1.2. Pathway sampling and transition states location

Reaction pathways were sampled with SSW-RS method[8] by using NN potential. The reaction pathways with given IS/FS pairs were connected by DESW method.[9] The force convergence criteria of IS/TS/FS during pathway was 0.01 eV/Å. Reaction pathways were further verified by extrapolating TS structures towards IS and FS directions. The relative energy of important initial structure (IS), transition structure (TS) and final structure (FS) were verified by hybrid functional HSE06.[10]

1.3 DFT calculations

All DFT calculation utilized was performed by using plane wave DFT code, VASP, where electron-ion interaction is represented by the projector augmented wave (PAW) pesudopotential.[11-12] The exchange functional utilized is the GGA-PBE[13] and hybrid HSE06[10]. Fro global dataset generation, the valence electrons (2p, 3d, 4s for Co; 2s, 2p for O) were expanded in a plane-wave basis set with a cutoff energy of 450 eV. All the key minima and transition states reported in the work were finally converged using 650 eV cutoff. The first Brillion zone k-point sampling utilizes an automated Monkhorst– Pack scheme with the mesh determined by 25 times of the reciprocal lattice vectors. The energy, force and stress criterion for convergence of the electron density and structure optimization were set at 10^{-6} eV, 0.01 eV/Å and 0.1 GPa, respectively. We used a Hubbard-like term (U_{eff}) describing the on-site Columbic interactions to improve the description of localized states for the Co *3d* orbital (U_{eff} = 3.5 eV).[14] The reason for using U_{eff} =3.5 eV is discussed in 1.4 below.

1.4 The sensitivity analysis of U values

The sensitivity of U value on the Co^{2+} and Co^{3+} is analyzed by benchmarking with experimental data and hybrid HSE06 calculations. The results are listed in Table S3. In general, the increase of U value leads to the increase of lattice parameters, causing the larger deviation of theoretical value from the experimental value. It means that the U value should not be too large. For the energetics, for example, our results show that the larger the U value, the more endothermic the formation of Co_3O_4 will be. The formation energy of Co_3O_4 agrees with the experimental value for U values in between the U value of 3 eV to 3.5 eV. For the band gap, the increase of U value leads to the increase of the band gap for c-CoO (Table S4). The band gap calculated by GGA+U is close to that calculated by HSE06 functional (3.2 eV) at the U value of 3.5 eV.

A significant number of publications on CoO_x using DFT+U approach. For example, the effect of U value on Co^{2+} and Co^{3+} (in CoO, Co_3O_4 and Co_2O_3) is studied by Singh et al.[15] The PBE+U calculated magnetic moment per Co site and the band gap as a function of U in a range between 1 eV to 8 eV is reported. Both the magnetic moment per Co site and the bandgap increase with the increase of U value. The magnetic moment per Co is relatively small with a U value below 3 eV in CoO, Co_3O_4 and Co_2O_3. The calculated bandgap overshoots the experimental value with a U value above 4 eV for CoO and Co_3O_4. They conclude that a U value between 3 eV and 4 eV is a sensible choice. Moreover, the value of U can also be learned by fitting the reaction energy for the oxidation of CoO to Co_3O_4 according to the equation 1, see Table S3:

$$6CoO + O_2 \rightarrow 2Co_3O_4 \quad (1)$$

Both the work by García-Mota et al,[16] and by Wang et al[17] suggests that the U value at 3.3 or 3.5 eV is close to the experimental value (in their calculations O_2 energy is corrected either by using the H_2O reference (García-Mota et al[16]) or by fitting the formation enthalpy of simple non-transition metal oxides (Wang et al[17])). From all evidences, we have concluded that a U value 3.5 is suitable for describing CoO_x practically.

Table S3 The calculated lattice parameters (Å) of c-CoO and Co_3O_4, formation energies of Co_3O_4 (eV/atom), the oxidation enthalpy from c-CoO to Co_3O_4 (eq1) and band gap (eV) of c-CoO with respect to U values.

	Lattice Parameters		**Formation Energy**	**Oxidation Enthalpy**		**Bandgap**
U value	c-CoO (a)	Co_3O_4 (a)	Co_3O_4	c-CoO → Co_3O_4		c-CoO
1	4.264	8.120	-3.385	--	--	1.2
2	4.275	8.134	-2.455	-6.06[a]	-5.9[b]	2.2
3	4.283	8.145	-1.593	-4.5 [a]	--	3.0
3.5(this work)	4.284	8.149	-1.181	--	--	3.2
4	4.285	8.153	-0.781	-2.92[a]	-3.13[b]	3.4
5	4.294	8.160	-0.009	-1.44[a]	--	3.4
Exp.	4.262 [c]	8.080[d]	-1.319	-3.68[e]	-3.68[e]	--
HSE cal.	--	--	--	--	--	3.2[f]

[a] calculated by García-Mota et al[16]

[b] calculated by Wang et al[17]

[c] experimental data are taken from Kannan et al[18]

[d] experimental data are taken from Gopalakrishnan et al[19]

[e] experimental data calculated from *Lange's Handbook of Chemistry*[20]

[f] Calculated by HSE06 functional

1.5 Phase diagram thermodynamics analysis

To determine the relative stability of CoO_x composites in Fig 2, the relative formation energy in forming CoO_x from pure hcp Co metal and O_2 is calculated. Thermodynamics analyses have been performed where the following formula is used to compute the formation enthalpy of Co_xO_y crystals.

$$x\ Co + (y/2)\ O_2 \dashrightarrow Co_xO_y \qquad (2)$$

To determine the formation enthalpy (***ΔH***) per atom for the above reactions, one needs to compute

$$\Delta H = H(Co_xO_y) - x\ H(Co) - (y/2)\ H(O_2) \qquad (3)$$

where H is the enthalpy of bulks/molecules. The $H[X]$ can be approximated by their DFT/NN total energy $E[X]$ with appropriate inclusion of zero-point-energy (***ZPE***), since it is known that the vibration entropy and the ***pV*** term contributions of solid phases are negligibly small.

The correction of the relative formation energy is established following the methodology of correcting relative formation energy calculated with GGA+U introduced by Jain et al. [21] For CoO (rock-salt) and Co_3O_4, we compute the energies of reactions of the form

$$M^{\square N} + \frac{x}{2} O_2^{fit} = MO_x^{NN} + \Delta H \qquad (4)$$

in which the experimental reaction enthalpy is obtained from Lange's Handbook of Chemistry [20]. It

is noticeable that during the global database generation the cobalt metal is computed in standard GGA, whereas the cobalt oxide is calculated in GGA+U. The correction ΔE_M is determined as the average difference between the experimental and computed formation enthalpy for CoO and Co_3O_4 (normalized per Co atom).

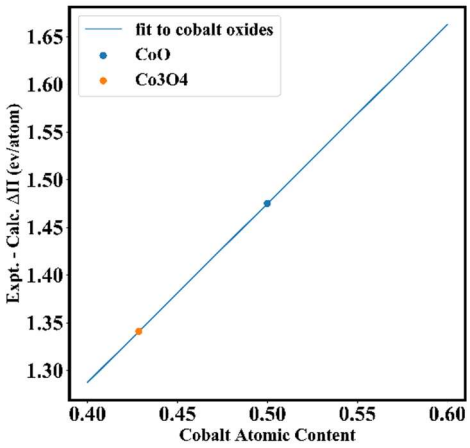

Figure S1 Differences between experimental and calculated and formation enthalpies as a function of metal content for Co. The blue line is fitted via least-squares to the CoO (the blue point) and Co_3O_4 (the orange point) data, and its slope represents the magnitude of the adjustment ΔE_M (ΔE_M (eV/atom) = 1.877 × Co% + 0.537)

1.6 Definition of distance-weighted Steinhart order parameter

The distance-weighted OP is defined as eq. (5)

$$\mathrm{OP}_l = \left(\frac{4\pi}{2l+1} \sum_{m=-l}^{l} \left| \frac{1}{N_{bonds}} \sum_{i \neq j} e^{-\frac{1}{2} \frac{r_{ij}-r_c}{r_c}} Y_{lm}(n) \right|^2 \right)^{\frac{1}{2}} \qquad (5)$$

where Y_{lm} is the spherical harmonic function of degree l and order m; n is the normalized direction between all bonded atoms; i and j are atoms in the lattice, r_{ij} is the distance between atom i and j, and r_c is set at 60% of the sum of the radius for i and j atoms (e.g. ~2.47 Å for a Co–O bond and r_c is 1.48 Å). N_{bonds} is the number of bonds (in the first bonding shell). By choosing a suitable degree l, the order parameter can measure the short- and medium-range ordering of atoms in the lattice.[22]

2. Band structure and Geometry for CoO phases

2.1 Band structure of c-CoO and h-CoO with different magnetic states

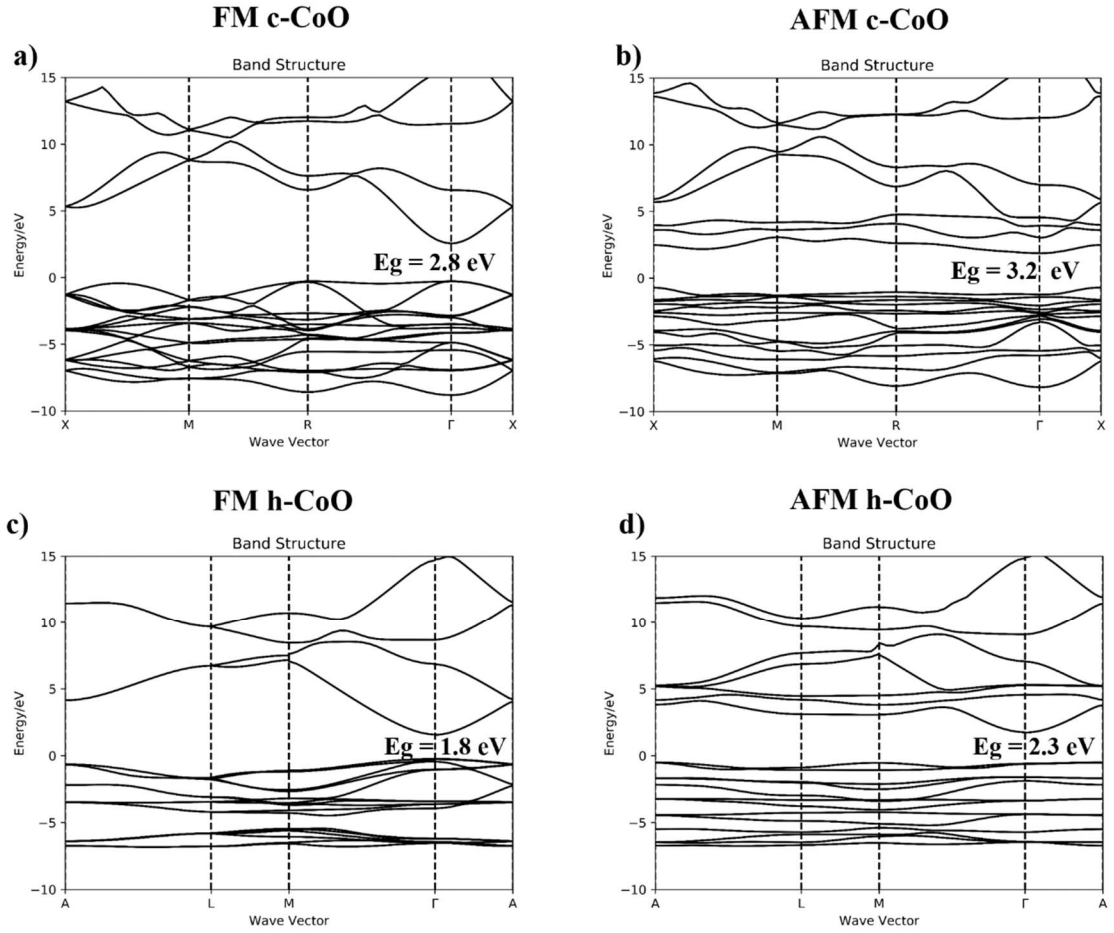

Figure S2 Energy band graph calculated with HSE06 of (**a**) ferromagnetic c-CoO; (**b**) anti-ferromagnetic c-CoO; (**c**) ferromagnetic h-CoO; (**d**) anti-ferromagnetic c-CoO.

2.2 CoO distinct minima sampled from the SSW-NN global search

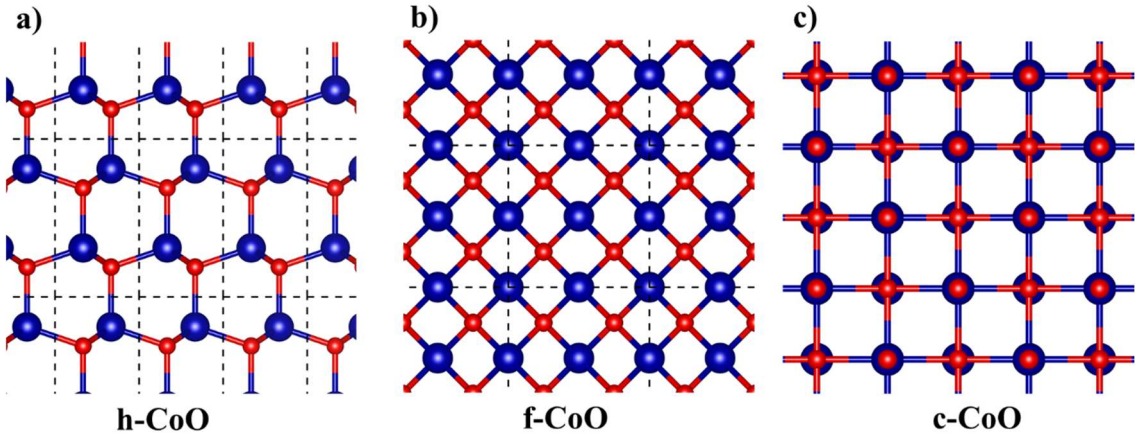

Figure S3 Three typical structures of CoO identified from the SSW-NN global search (**a**), (**b**) and (**c**) are related to wurtzite CoO (c-CoO), zinc-blende CoO (f-CoO) and rock-salt CoO (c-CoO), respectively. There relative positions in the global PES are mentioned in Figure 1.

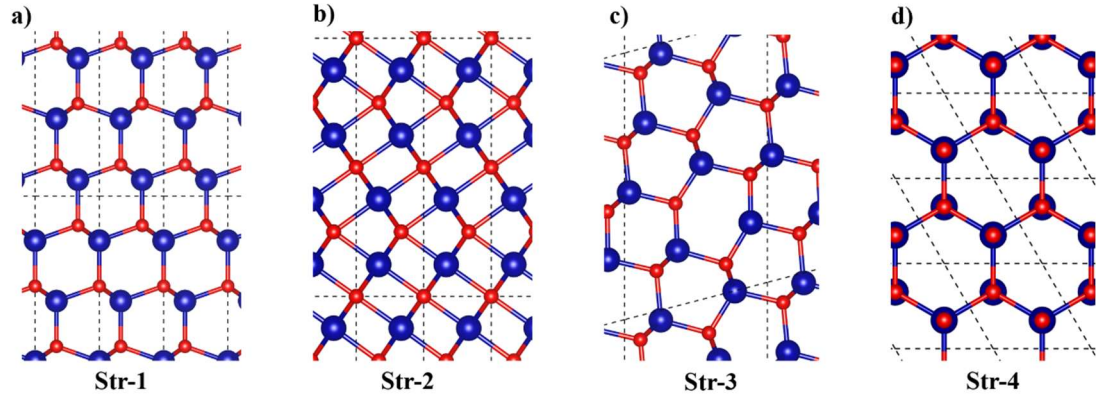

Figure S4 Four structures identified from the SSW-NN global search. (**a**), (**b**), (**c**) and (**d**) are related to CoO-Str1, CoO-Str2, CoO-Str3 and CoO-Str4 mentioned in Figure 1, respectively. CoO-Str1 has a mixed structure of wurtzite CoO and zinc-blende CoO. CoO-Str2 is a phase junction structure of c-CoO. CoO-Str3 is a mixture of wurtzite CoO and zinc-blende CoO with stacking fault. CoO-Str4 has an AA stack graphene-type structure.

3. Co_2O_3

3.1 Energy of Co_2O_3 distinct minima sampled from SSW-NN global search

Table S4. Energy (meV/atom) of Co_2O_3 distinct minima sampled from SSW-NN global search. the Relative energy is calculated from PBE+U (U = 3.5 eV)

	PBE+U-en	NN-en	en-diff	Relative Energy
Str-GM	-5.55	-5.55	0.37	0.00
Str-SLM	-5.54	-5.54	-2.55	15.44
Str-1	-5.54	-5.54	0.19	16.32
Str-2	-5.53	-5.52	-4.91	25.74
Str-3	-5.52	-5.52	0.05	37.54

3.2 Phase transition pathway of Co_2O_3 global minima and second lowest minima

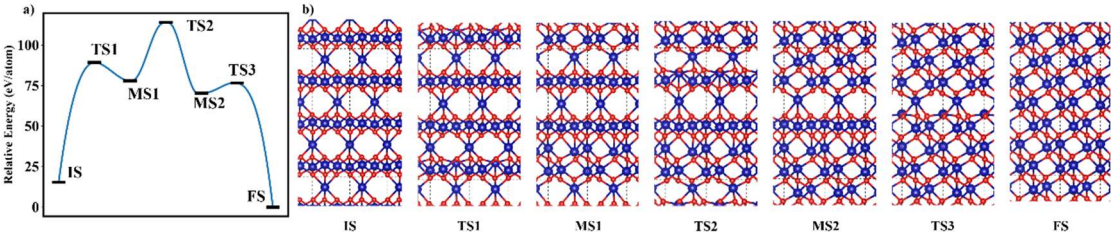

Figure S5 (**a**) Potential energy profile for phase transition pathway between Co_2O_3-GM and Co_2O_3-SLM. The corresponding reaction snapshots are shown in (**b**).

The lowest energy pathway of phase transition between Co_2O_3-GM and Co_2O_3-SLM is shown in Figure S5. Co_2O_3-SLM has a layered structure in which CoO_2 layer has a MoS_2 structure. The interlayer six-coordinated Co ions connect different CoO_2 layers. During the phase transition from Co_2O_3-SLM to Co_2O_3-GM, 1/3 Co atoms in one CoO_2 layer migrate into the neighboring interlayer. A layered changing style can be found from the reaction snapshots shown in Figure S5 b.

4. Optimized XYZ positions for wurtzite CoO, rock-salt CoO and transition state on their phase transition pathway

VASP POSCAR format

POSCAR (wurtzite CoO)
1.00000000000000
5.7020110500000003 0.0000000000000000 0.0000000000000000
-0.0027944963917192 6.5809650466820226 0.0000000000000000
-0.0000000288664519 0.0000001517694165 5.3352445399999979
Co O
8 8
Direct
0.6841950000000026 0.2646349999999984 0.1894270000000020
0.5181389999999979 0.5150119999999987 0.6894599999999969
0.1842109999999977 0.0146889999999971 0.1894599999999969
0.0181550000000001 0.2650649999999999 0.6894270000000020
0.6841950000000026 0.7646349999999984 0.1894270000000020
0.5181389999999979 0.0150119999999987 0.6894599999999969
0.1842109999999977 0.5146889999999971 0.1894599999999969
0.0181550000000001 0.7650649999999999 0.6894270000000020
0.6847420000000000 0.2649710000000027 0.8105550000000008
0.5175860000000014 0.5147019999999998 0.3105580000000003
0.1847640000000013 0.0149990000000031 0.8105580000000003
0.0176080000000027 0.2647290000000027 0.3105550000000008
0.6847420000000000 0.7649710000000027 0.8105550000000008
0.5175860000000014 0.0147019999999998 0.3105580000000003
0.1847640000000013 0.5149990000000031 0.8105580000000003
0.0176080000000027 0.7647290000000027 0.3105550000000008

POSCAR (rock-salt CoO)
1.00000000000000
4.0945313126641203 -5.4550516698763003 0.0019246347879946
2.7290545547908986 5.4556160519476515 -0.0011398703388338
0.0005281278407222 -0.0014546380281674 4.2927706893267299
Co O
8 8
Direct
0.7261740000000003 0.9281780000000026 0.2501120000000014
0.4764109999999988 0.0535539999999983 0.7501990000000021
0.2260119999999972 0.1785399999999981 0.2499109999999973
0.9761969999999991 0.3036049999999975 0.7498259999999988
0.7262160000000009 0.4285769999999971 0.2499279999999970
0.4763200000000012 0.5537350000000032 0.7500050000000016
0.2260500000000008 0.6783619999999999 0.2501609999999985
0.9760810000000006 0.8036099999999990 0.7499150000000014
0.7262300000000010 0.9262330000000034 0.7498300000000029
0.4762020000000007 0.0512829999999980 0.2498450000000005
0.2262180000000029 0.1807670000000030 0.7500690000000034
0.9761430000000004 0.3057510000000008 0.2501010000000008
0.7260929999999988 0.4263789999999972 0.7501329999999982
0.4761889999999980 0.5513720000000006 0.2499480000000034
0.2261469999999974 0.6806709999999967 0.7499030000000033
0.9761209999999991 0.8057879999999997 0.2501150000000010

POSCAR (transition state on phase transition pathway of wurtzite CoO and rock-salt CoO)
1.00000000000000

6.3972675386360081	-0.0184204226539554	0.0000023332731315
1.6243465869313283	6.1883354402825068	0.0000228273196109
0.0000116483722025	0.0000315400268682	4.4802921715273465

Co O
8 8
Direct

0.7015439999999984	0.2392139999999969	0.2328649999999968
0.5008570000000034	0.5402410000000017	0.7328260000000029
0.2014929999999993	0.9894589999999965	0.2328260000000029
0.0008070000000018	0.2904860000000014	0.7328649999999968
0.7015439999999984	0.7392139999999969	0.2328649999999968
0.5008570000000034	0.0402410000000017	0.7328260000000029
0.2014929999999993	0.4894589999999965	0.2328260000000029
0.0008070000000018	0.7904860000000014	0.7328649999999968
0.7056290000000018	0.2331089999999989	0.7671559999999999
0.4967820000000032	0.5463799999999992	0.2671530000000004
0.2055679999999995	0.9833199999999991	0.7671530000000004
0.9967210000000009	0.2965909999999994	0.2671559999999999
0.7056290000000018	0.7331089999999989	0.7671559999999999
0.4967820000000032	0.0463799999999992	0.2671530000000004
0.2055679999999995	0.4833199999999991	0.7671530000000004
0.9967210000000009	0.7965909999999994	0.2671559999999999

5. Optimized XYZ positions for Co_3O_4, $CoO_{1.05}$, $CoO_{1.1}$, $CoO_{1.2}$ and $CoO_{1.4}$

VASP POSCAR format

POSCAR (Co3O4)
1.00000000
5.76719 0.00000 0.00000
-2.88325 9.56249 0.00000
-2.88325 -0.86952 4.91822
Co O
12 16
Direct
0.935152 0.508960 0.810665
0.435154 0.258960 0.560663
0.935147 0.258961 0.060667
0.935156 0.008962 0.310667
0.560114 0.946432 0.623156
0.435154 0.758961 0.060669
0.310194 0.071487 0.998176
0.560103 0.446432 0.123150
0.935151 0.258961 0.560662
0.935160 0.758959 0.560665
0.935156 0.758959 0.060670
0.310202 0.571490 0.498180
0.171298 0.140900 0.650996
0.699011 0.154760 0.692595
0.171296 0.640899 0.151000
0.699010 0.377021 0.470331
0.699022 0.877021 0.414867
0.699011 0.654759 0.192596
0.143539 0.377019 0.914862
0.699009 0.877022 0.970337
0.143547 0.877020 0.414859
0.171294 0.863160 0.928734
0.726766 0.640900 0.706471
0.171285 0.140902 0.206462
0.726761 0.140903 0.206472
0.699010 0.377019 0.914861
0.171296 0.640900 0.706472

0.171297 0.363162 0.428737

POSCAR (CoO1.05)
1.00000000
5.68679 0.00000 0.00000
-0.96474 13.49378 0.00000
-0.00018 -0.80487 6.54113
Co O
20 21
Direct
0.791644 0.015056 0.382511
0.849550 0.415447 0.982614
0.217623 0.614332 0.535182
0.348269 0.412216 0.732141
0.915509 0.810732 0.086587
0.152060 0.207771 0.430816
0.651087 0.215184 0.680447
0.420844 0.816985 0.833456
0.140329 0.210953 0.932181
0.853045 0.413991 0.483641
0.763984 0.010458 0.881739
0.717228 0.610182 0.281572
0.650917 0.215841 0.185445
0.283736 0.008132 0.638839
0.218100 0.614092 0.030172
0.714345 0.614336 0.782075
0.346477 0.413398 0.233282
0.416368 0.806830 0.331062
0.283851 0.008163 0.123550
0.915149 0.811103 0.577205
0.889146 0.659352 0.542408
0.831871 0.264763 0.445805
0.821912 0.266700 0.945178
0.689834 0.463126 0.744372
0.392433 0.666089 0.795612
0.193197 0.463436 0.496328
0.192295 0.462989 0.993936
0.889098 0.658889 0.044889
0.320699 0.262819 0.694049
0.789143 0.856914 0.843566
0.248559 0.849879 0.106628
0.754138 0.862600 0.344590
0.439625 0.960616 0.869324
0.638708 0.070163 0.159948
0.135802 0.058165 0.393656
0.392671 0.656475 0.293204

0.320049	0.263142	0.195861
0.086013	0.064613	0.895290
0.248438	0.849870	0.576801
0.638741	0.069730	0.632912
0.690514	0.459896	0.245113

POSCAR (CoO1.1)

1.00000000

3.29327 0.00000 0.00000

0.00040 5.70411 0.00000

-0.00772 -0.00120 26.98573

Co O

20 22

Direct

0.064772 0.886556 0.284228

0.067999 0.886438 0.776020

0.565314 0.720244 0.481541

0.567998 0.386439 0.776020

0.065211 0.553393 0.184845

0.568115 0.720053 0.874350

0.567158 0.720010 0.676516

0.568296 0.386744 0.974494

0.065316 0.220245 0.481541

0.066319 0.553491 0.580923

0.565212 0.053393 0.184845

0.564773 0.386556 0.284228

0.067653 0.220364 0.079231

0.068139 0.220053 0.874350

0.566322 0.053492 0.580923

0.565034 0.053295 0.383482

0.067162 0.220010 0.676516

0.065033 0.553296 0.383482

0.068352 0.886744 0.974494

0.567652 0.720364 0.079231

0.567150 0.053347 0.665149

0.565056 0.719983 0.405362

0.067712 0.887029 0.044125

0.068074 0.886689 0.851156

0.568229 0.720092 0.947760

0.565447 0.386756 0.211291

0.564835 0.053237 0.308629

0.064835 0.553237 0.308629

0.065447 0.886756 0.211291

0.066325 0.220162 0.589657

0.567914 0.719789 0.755217

0.567654 0.053716 0.115278

0.065057 0.219983 0.405362

0.565419 0.053563 0.500986

0.065416 0.553563 0.500986

0.566322 0.720162 0.589657

0.067649	0.553716	0.115278
0.067146	0.553346	0.665148
0.568080	0.386690	0.851156
0.068202	0.220092	0.947760
0.567702	0.387029	0.044125
0.067916	0.219790	0.755217

POSCAR (CoO1.2)
1.00000000
5.91615 0.00000 0.00000
0.00000 6.00268 0.00000
-2.95804 3.00134 12.55823
Co O
20 24
Direct
0.130549 0.286519 0.280905
0.130491 0.786792 0.780883
0.972271 0.933672 0.964439
0.590074 0.577077 0.199948
0.972313 0.456317 0.964523
0.790456 0.120348 0.600775
0.630491 0.786793 0.780882
0.630497 0.286837 0.780883
0.130526 0.786542 0.280859
0.804580 0.113715 0.126701
0.456479 0.459531 0.435064
0.130497 0.286838 0.780881
0.470546 0.940247 0.960989
0.470555 0.453190 0.961007
0.288689 0.639950 0.597243
0.671006 0.996140 0.361817
0.790447 0.633309 0.600758
0.302284 0.113716 0.126699
0.958774 0.459531 0.435064
0.288729 0.117223 0.597324
0.548585 0.868729 0.616958
0.709871 0.670891 0.439549
0.348245 0.534660 0.284611
0.916565 0.534660 0.284611
0.879716 0.524325 0.779324
0.381262 0.049344 0.782416
0.727803 0.193825 0.966786
0.212492 0.704809 0.944807
0.381273 0.522767 0.782438
0.551191 0.329560 0.122216
0.709876 0.243683 0.439559
0.207199 0.668705 0.434206
0.344511 0.038389 0.277152
0.048503 0.868729 0.616958
0.041916 0.379720 0.594979
0.912833 0.038388 0.277154

0.712411	0.704810	0.944806
0.533217	0.379720	0.594979
0.053835	0.904561	0.127505
0.879729	0.050878	0.779351
0.551186	0.902363	0.122205
0.053862	0.322032	0.127559
0.207226	0.251182	0.434258
0.219103	0.193825	0.966785

POSCAR (CoO1.4)

1.00000000

5.74237 0.00000 0.00000

-0.00814 5.79245 0.00000

-1.42553 -1.46215 14.03913

Co O

20 28

Direct

0.563866 0.132489 0.606513

0.204040 0.783716 0.174356

0.777317 0.346089 0.461298

0.563866 0.632489 0.606513

0.923691 0.481262 0.038671

0.508816 0.827855 0.389471

0.082269 0.401511 0.680196

0.991830 0.557780 0.315959

0.136575 0.204180 0.896573

0.045463 0.863466 0.532831

0.421027 0.484184 0.036188

0.706705 0.780793 0.176839

0.991157 0.060798 0.316454

0.472910 0.282883 0.240304

0.654822 0.982095 0.972723

0.135901 0.707198 0.897067

0.278460 0.345794 0.461206

0.618915 0.437122 0.823556

0.350415 0.918888 0.751729

0.849272 0.919183 0.751820

0.343687 0.884051 0.614549

0.026403 0.565074 0.453158

0.910100 0.953695 0.888202

0.101329 0.699903 0.759868

0.769906 0.311398 0.324833

0.339735 0.380436 0.598464

0.170932 0.701736 0.035758

0.787997 0.884541 0.614563

0.026077 0.123727 0.454418

0.675692 0.707544 0.042267

0.784045 0.380926 0.598478

0.217632 0.311283 0.324824

0.529609 0.126007 0.469667

0.598122 0.138971 0.743359

0.670972 0.277746 0.040887

0.172141 0.264955 0.029707

0.452040	0.557434	0.170759
0.955590	0.000022	0.183319
0.956799	0.563242	0.177268
0.918064	0.455755	0.902325
0.771416	0.807933	0.312392
0.209668	0.809222	0.310702
0.357826	0.953579	0.888193
0.456760	0.987232	0.172140
0.101655	0.141250	0.758608
0.529956	0.570263	0.469618
0.356315	0.457045	0.900634
0.597776	0.694714	0.743408

6. Optimized XYZ positions for global minima and second lowest minima of Co_2O_3

VASP POSCAR format

POSCAR (global minima of Co_2O_3)
1.00000000
4.80594 0.00000 0.00000
-2.40242 4.16376 0.00000
-0.00089 0.00081 13.07997
Co O
12 18
Direct
0.800051 0.400265 0.880882
0.466607 0.733284 0.352423
0.133215 0.066395 0.714210
0.800153 0.400329 0.185825
0.466492 0.732817 0.547528
0.133479 0.067116 0.019126
0.133226 0.066199 0.519116
0.799865 0.399597 0.685804
0.466874 0.733791 0.047573
0.133399 0.066937 0.214182
0.466703 0.733452 0.852479
0.799990 0.399822 0.380875
0.768205 0.035111 0.949997
0.498479 0.400051 0.283325
0.133193 0.764713 0.616689
0.165234 0.733760 0.949987
0.799934 0.098542 0.283296
0.434654 0.367613 0.616636
0.466832 0.432249 0.950049
0.101442 0.701736 0.283344
0.831559 0.066134 0.616664
0.101558 0.399871 0.783359
0.832026 0.765467 0.116672
0.466697 0.034589 0.450012
0.799793 0.701326 0.783273
0.435136 0.067210 0.116663
0.165145 0.431437 0.449955

0.498492	0.098586	0.783387
0.133504	0.368584	0.116678
0.768065	0.733016	0.449992

POSCAR(second lowest minima of Co_2O_3)

1.00000000

4.90695	0.00000	0.00000
2.45295	4.24970	0.00000
-0.01554	-0.00640	14.49438

Co O

12 18

Direct

0.032218	0.667377	0.916594
0.367666	0.999297	0.250059
0.700167	0.333405	0.583344
0.366394	0.000075	0.074618
0.702129	0.331993	0.408040
0.031555	0.667874	0.741190
0.368724	0.998775	0.425484
0.698071	0.334680	0.758654
0.033122	0.666626	0.092013
0.699761	0.333350	0.083312
0.364931	0.001286	0.749912
0.035293	0.665337	0.416773
0.708919	0.980797	0.818355
0.043884	0.312814	0.151769
0.379339	0.644898	0.485169
0.041702	0.345281	0.818332
0.376648	0.677313	0.151746
0.712187	0.009344	0.485212
0.344403	0.678084	0.818348
0.679397	0.010085	0.151756
0.014915	0.342176	0.485239
0.020947	0.021676	0.681527
0.355658	0.353881	0.014855
0.691287	0.685871	0.348329
0.688065	0.657292	0.681479
0.022869	0.989413	0.014878
0.358527	0.321357	0.348352
0.385278	0.324449	0.681461
0.720118	0.656621	0.014857
0.055824	0.988571	0.348343

References

1. Shang, C.; Liu, Z.-P. Stochastic Surface Walking Method for Structure Prediction and Pathway Searching. *J. Chem. Theory Comput.* **2013,** *9*, 1838-1845.
2. Zhang, X.-J.; Shang, C.; Liu, Z.-P. From Atoms to Fullerene: Stochastic Surface Walking Solution for Automated Structure Prediction of Complex Material. *J. Chem. Theory Comput.* **2013,** *9*, 3252-3260.
3. Guan, S.-H.; Zhang, X.-J.; Liu, Z.-P. Energy Landscape of Zirconia Phase Transitions. *J. Am. Chem. Soc.* **2015,** *137*, 8010-8013.
4. Zhu, S.-C.; Xie, S.-H.; Liu, Z.-P. Nature of Rutile Nuclei in Anatase-to-Rutile Phase Transition. *J. Am. Chem. Soc.* **2015,** *137*, 11532-11539.
5. Li, Y.-F.; Zhu, S.-C.; Liu, Z.-P. Reaction Network of Layer-to-Tunnel Transition of Mno2. *J. Am. Chem. Soc.* **2016,** *138*, 5371-5379.
6. Huang, S.-D.; Shang, C.; Zhang, X.-J.; Liu, Z.-P. Material Discovery by Combining Stochastic Surface Walking Global Optimization with a Neural Network. *Chem. Sci.* **2017,** *8*, 6327-6337.
7. Huang, S.-D.; Shang, C.; Kang, P.-L.; Liu, Z.-P. Atomic Structure of Boron Resolved Using Machine Learning and Global Sampling. *Chem. Sci.* **2018,** *9*, 8644-8655.
8. Zhang, X.-J.; Liu, Z.-P. Reaction Sampling and Reactivity Prediction Using the Stochastic Surface Walking Method. *Phys. Chem. Chem. Phys.* **2015,** *17*, 2757-2769.
9. Zhang, X.-J.; Shang, C.; Liu, Z.-P. Double-Ended Surface Walking Method for Pathway Building and Transition State Location of Complex Reactions. *J. Chem. Theory Comput.* **2013,** *9*, 5745-5753.
10. Krukau, A. V.; Vydrov, O. A.; Izmaylov, A. F.; Scuseria, G. E. Influence of the Exchange Screening Parameter on the Performance of Screened Hybrid Functionals. *J. Chem. Phys.* **2006,** *125*, 224106.
11. Blöchl, P. E. Projector Augmented-Wave Method. *Phys. Rev. B: Condens. Matter Mater. Phys.* **1994,** *50*, 17953-17979.
12. Kresse, G.; Joubert, D. From Ultrasoft Pseudopotentials to the Projector Augmented-Wave Method. *Phys. Rev. B: Condens. Matter Mater. Phys.* **1999,** *59*, 1758-1775.
13. Perdew, J. P.; Burke, K.; Ernzerhof, M. Generalized Gradient Approximation Made Simple. *Phys. Rev. Lett.* **1996,** *77*, 3865-3868.
14. Yaresko, A. Electronic Band Structure and Exchange Coupling Constants in Acr2x4 Spinels (a= Zn, Cd, Hg; X= O, S, Se). *Phys. Rev. B* **2008,** *77*, 115106.
15. Singh, V.; Major, D. T. Electronic Structure and Bonding in Co-Based Single and Mixed Valence Oxides: A Quantum Chemical Perspective. *Inorganic Chemistry* **2016,** *55*, 3307-3315.
16. García-Mota, M.; Bajdich, M.; Viswanathan, V.; Vojvodic, A.; Bell, A. T.; Nørskov, J. K. Importance of Correlation in Determining Electrocatalytic Oxygen Evolution Activity on Cobalt Oxides. *J. Phys. Chem. C* **2012,** *116*, 21077-21082.
17. Wang, L.; Maxisch, T.; Ceder, G. Oxidation Energies of Transition Metal Oxides within the Gga+ U Framework. *Phys. Rev. B* **2006,** *73*, 195107.
18. Kannan, R.; Seehra, M. S. Percolation Effects and Magnetic Properties of the Randomly Diluted Fcc System ${\Mathrm{Co}}_{\Mathrm{P}}$${\Mathrm{Mg}}_{1\Mathrm{\Ensuremath{-}}\Mathrm{P}}$O. *Phys. Rev. B* **1987,** *35*, 6847-6853.
19. Gopalakrishnan, J.; Appandairajan, N. K.; Viswanathan, B. Co3-Xznxo4 ($0 \leq X \leq 1$) Spinel Oxides. *Proceedings of the Indian Academy of Sciences - Chemical Sciences* **1979,** *88*, 217-222.

20. Dean, J. A. *Lange's Handbook of Chemistry*. New york; London: McGraw-Hill, Inc.: 1999.

21. Jain, A.; Hautier, G.; Ong, S. P.; Moore, C. J.; Fischer, C. C.; Persson, K. A.; Ceder, G. Formation Enthalpies by Mixing Gga and Gga+ U Calculations. *Phys. Rev. B* **2011,** *84*, 045115.

22. Zhang, X.-J.; Shang, C.; Liu, Z.-P. Pressure-Induced Silica Quartz Amorphization Studied by Iterative Stochastic Surface Walking Reaction Sampling. *Phys. Chem. Chem. Phys.* **2017,** *19*, 4725-4733.